JVI
Journals.ASM.org

Ex Vivo and *In Vivo* Inhibition of Human Rhinovirus Replication by a New Pseudosubstrate of Viral 2A Protease

Nisrine Falah,[a] Sébastien Violot,[b] Didier Décimo,[c] Fatma Berri,[a] Marie-Laure Foucault-Grunenwald,[a] Théophile Ohlmann,[c] Isabelle Schuffenecker,[d] Florence Morfin,[d] Bruno Lina,[a,d] Béatrice Riteau,[a,e] and Jean-Claude Cortay[a]

VirPath, EMR 4610, Virologie et Pathologie Humaine, Université Lyon 1, Université de Lyon, Faculté de Médecine Lyon-Est, Secteur Laennec, Lyon, France[a]; Biocristallographie et Biologie Structurale des Cibles Thérapeutiques, Université Lyon 1, Université de Lyon, Lyon, France, and CNRS, UMR 5086, Bases Moléculaires et Structurales des Systèmes Infectieux, Vercors, France[b]; Ecole Normale Supérieure de Lyon, Unité de Virologie Humaine, INSERM U758, Université Lyon 1, Université de Lyon, Lyon, France[c]; Laboratoire de Virologie, Hospices Civils de Lyon, Lyon, France[d]; and INRA, Tours, France[e]

Human rhinoviruses (HRVs) remain a significant public health problem as they are the major cause of both upper and lower respiratory tract infections. Unfortunately, to date no vaccine or antiviral against these pathogens is available. Here, using a high-throughput yeast two-hybrid screening, we identified a 6-amino-acid hit peptide, LVLQTM, which acted as a pseudosubstrate of the viral 2A cysteine protease (2A^{pro}) and inhibited its activity. This peptide was chemically modified with a reactive electrophilic fluoromethylketone group to form a covalent linkage with the nucleophilic active-site thiol of the enzyme. *Ex vivo* and *in vivo* experiments showed that thus converted, LVLQTM was a strong inhibitor of HRV replication in both A549 cells and mice. To our knowledge, this is the first report validating a compound against HRV infection in a mouse model.

Human rhinoviruses (HRVs) belong to the enterovirus group of the *Picornaviridae* family and are the main causative agents of the common cold, asthma exacerbations, and chronic obstructive pulmonary disease in humans (22). To date, there is no vaccine against HRV as there is almost no cross protection between the nearly 100 serotypes identified so far (21). Furthermore, no antiviral treatment against HRV is currently available on the market. Thus, there is an urgent need for validation of new compounds against HRV.

Among several antiviral strategies attempting to impair rhinovirus replication, one consists of blocking the activity of the viral HRV 2A protease (2A^{pro}). Targeting 2A^{pro} is of particular interest as it is a cysteine protease playing multifunctional roles necessary for viral replication. These roles include (i) autoprocessing by *cis* cleavage at the VP1-2A^{pro} junction; (ii) inhibition of the host cell translation through cleavage of the initiation factor eIF4G (17, 27) and the poly(A)-binding protein (PABP) (10); (iii) contribution to the deleterious overwhelming host cellular defense (3, 9, 23); and (iv) strengthening of viral polysome formation and stability (11, 12).

Several 2A^{pro} inhibitors have already been described and include alkylating agents such as iodoacetamide or *N*-ethylmaleimide that can react with the catalytic cysteine of the enzyme and that have been shown to reduce 2A^{pro} activity (15). Moreover, as the substrate-binding pocket of elastase is similar to that of 2A^{pro}, two substrate-derived elastase inhibitors, elastinal and methoxysuccinyl-Ala-Ala-Pro-Val-chloromethylketone have been reported to inhibit the *in vitro* proteolytic activity of 2A^{pro} and consequently reduce viral yields of HRV type 14 (HRV-14) and poliovirus type 1 (PV-1) (18). Furthermore, it has been demonstrated that the irreversible caspase inhibitor benzyloxycarbonyl-Val-Ala-Asp(methoxy)-fluoromethylketone (z-VAD-fmk) (7) is also able to directly inactivate HRV and coxsackie B virus type 4 (CBV4) 2A^{pro} enzymes (5). However, none of these compounds has ever been tested *in vivo*, thus impairing the validation of their efficacy in preclinical assays and the possibility to go further in the development of anti-HRV therapies.

The aim of this study was to design a peptide inhibitor of HRV-2 2A^{pro} and to test its antiviral activity *ex vivo* in A549 cells and *in vivo* in mice which are susceptible to infection by the minor HRV group member HRV-2.

Here, we report the identification of the LVLQTM peptide as a decoy substrate for 2A^{pro} that blocked enzyme activity upon binding and consequently affected HRV-2 replication *ex vivo* and *in vivo* when administered to infected mice. This is the first study validating such a compound *in vivo* in mice, opening new prospects for testing other drugs.

MATERIALS AND METHODS

Ethics statement. Experiments were performed according to recommendations of the National Commission of Animal Experiment (CNEA) and the National Committee on the Ethic Reflexion of Animal Experiments (CNREEA). The protocol was approved by the Committee of Animal Experiments of the University Claude Bernard Lyon I (permit number BH2008-13). All animal experiments were also carried out under the authority of a license issued by la Direction des Services Vétérinaires (accreditation number 78-114). All efforts were made to minimize suffering.

Yeast two-hybrid analysis. Yeast two-hybrid screening was performed by Hybrigenics, S.A., Paris, France. The full-length coding sequence for HRV-2 2A^{pro} (GenBank accession number X02316) was amplified by PCR and cloned into pB27 plasmid as a C-terminal fusion to LexA (LexA-p2A). The construct was validated by sequencing and used as bait to screen a random-primed human placenta cDNA library constructed into pP6 plasmid. pB27 and pP6 plasmids were derived from the original pBTM116 and pGADGH plasmids, respectively (34).

A total of 53.1 million clones (6-fold the complexity of the library) were screened using a mating approach with Y187 (*mat*α) and L40ΔGal4

Received 31 May 2011 Accepted 21 October 2011
Published ahead of print 9 November 2011
Address correspondence to Jean-Claude Cortay, cortay@univ-lyon1.fr.

doi:10.1128/JVI.05263-11

(*mat***a**) *Saccharomyces cerevisiae* yeast strains, as previously described (6). Fifty-one His-positive (His^+) colonies were selected on a medium lacking tryptophan, leucine, and histidine and supplemented with 100 mM 3-aminotriazole to suppress bait autoactivation. The prey fragments of the positive clones were then amplified by PCR and sequenced at their 5′ and 3′ junctions. The resulting sequences were used to identify the corresponding interacting proteins in the GenBank database (NCBI) using a fully automated procedure.

Bacterial expression vectors and protein purification. Synthetic genes (Eurofins MWG Operon) coding for HRV-2 $2A^{pro}$ or echovirus 6 (EV-6) $2A^{pro}$ (GenBank accession number AY302558) were cloned between the NdeI and XhoI sites of the pSCodon1.2 vector (Eurogentec) in fusion with either a Strep●Tag (WSHPQFEK) or a $(His)_6$ tag at their C termini. Recombinant plasmids were used to transform the *Escherichia coli* B SE1 strain [F^- Cm^r *ompT lon hsdSB* (r_B^- m_B^-) *gal dcm* (DE3) (*lacI*, T7 polymerase under the control of the PlacUV5 promoter) *ccdB*$^+$]. Bacteria were grown in the autoinduction medium ZYP-5052 (30) at 37°C for 5 to 6 h with vigorous shaking in baffled flasks, before growing to saturation at 20°C within 16 to 18 h. Subsequent purification steps were performed at 4°C. Cells were lysed with BugBuster protein extraction reagent (Novagen), and clarified supernatants were applied to the corresponding affinity chromatography resins. Strep●Tag proteins were purified using a Streptrap HP resin (GE Healthcare) and His-tagged proteins were purified using a HIS-Select HF nickel resin (Sigma) according to the respective manufacturers' instructions. In each case, proteins were dialyzed against buffer D (100 mM Tris-HCl, pH 7.5, 200 mM NaCl, 4 mM dithiothreitol [DTT]) and concentrated using a Vivaspin centrifugal concentrator device (Sartorius Stedim Biotech). Enzymes were stored at −20°C in buffer D containing 50% glycerol.

***In vitro* cleavage assays.** Different protease recognition site-coding sequences were inserted between the NheI and BglII sites in a short polypeptide linker that connects the native N and C termini of a circularly permuted firefly luciferase in the pGloSensor-10F linear vector (Promega). The resulting plasmids were then used as templates in a cell-free system for the expression of the corresponding GloSensor proteins containing the protease sites of interest. *In vitro* transcription/translation reactions were carried out in a TNT SP6 high-yield wheat germ master mix (Promega) supplemented with [^{35}S]methionine according to the manufacturer's protocol. Reaction mixtures were incubated for 2 h at 25°C. Two micrograms of recombinant tobacco etch virus (TEV) protease, HRV-2 $2A^{pro}$, or EV-6 $2A^{pro}$ was added to 13 μl of the *in vitro* translation reaction mixture and 13 μl of 2× digestion buffer (100 mM Tris-HCl, pH 8, 1 mM EDTA, 4 mM DTT [for TEV protease], 100 mM HEPES-NaOH, pH 7.9, 200 mM NaCl, 2 mM EDTA, 10 mM DTT [for HRV-2 $2A^{pro}$], 100 mM Tris-HCl, pH 7.5, 300 mM NaCl, and 10 mM DTT [for EV-6 $2A^{pro}$]) and incubated for 45 min at 30°C. Aliquots of total proteins were removed 0, 15, 30, and 45 min postincubation and separated in a 12% SDS-polyacrylamide gel. Autoradiography was performed after fluorography treatment. The 61-kDa band intensity was determined by densitometric analysis after background subtraction using Bio-Rad Quantity One one-dimension software. Luminescence detection was performed by diluting the remaining volume of each protease digestion and negative-control reaction mixture 1:20 in nuclease-free water, and 100 μl of these dilutions was added to each well of a white, flat-bottom 96-well plate. Each reaction was analyzed in triplicate. After addition of 100 μl Bright-Glo assay reagent to each well and incubation for 2 to 5 min at room temperature, luminescence was measured using a GloMax 96-well microplate luminometer. According to the manufacturer's instructions, the fold activation of each luciferase activity was calculated as follows: [(luminescence from tube A) − (luminescence from tube C)]/[(luminescence from tube B) − (luminescence from tube D)], where tube A contains a Plus-DNA TNT reaction mixture and HRV-2 $2A^{pro}$, tube B contains a Plus-DNA TNT reaction mixture only, tube C contains a no-DNA TNT reaction mixture and HRV-2 $2A^{pro}$, and tube D contains a no-DNA TNT reaction mixture only.

Pulldown experiments. For His pulldown assays, a PCR-amplified fragment corresponding to truncated proteins consisting of the C-terminal part (amino acids 274 to 520) of the functionally uncharacterized RBM6Δ6 protein ($RBM6\Delta6_{274\text{-}520}$) or $RBM6_{274\text{-}660}$ was inserted into the NcoI-XhoI sites of the expression vector pET-28 (Novagen). Translated proteins were synthesized *in vitro* using a T7 RNA polymerase-based TNT-coupled reticulocyte lysate system (Promega). HRV-2 $2A^{pro}$–$(His)_6$ fusion protein was bound to nickel nitrilotriacetic acid (Ni-NTA) magnetic agarose beads (Qiagen) and incubated for 1 h with 50 μl *in vitro*-translated [^{35}S]methionine-labeled $RBM6\Delta6_{274\text{-}520}$ or $RBM6_{274\text{-}660}$ in a total volume of 1 ml of incubation buffer (25 mM sodium phosphate, pH 8.0, 500 mM NaCl, 20 mM imidazole, and 0.005% Tween 20). Resin was collected with a magnetic separator and washed twice with 500 μl incubation buffer. Washed beads were resuspended in 40 μl of 2× SDS sample buffer, heated for 5 min, and pelleted in a microcentrifuge. Proteins from the supernatant were then subjected to a 12% SDS-PAGE. Gels were treated with Amplify reagent (GE Healthcare) for fluorography or subjected to Western blot analysis using a polyclonal antihistidine antibody (Cell Signaling). The amount of labeled proteins which coeluted with HRV-2 $2A^{pro}$-$(His)_6$ was quantified by densitometric analysis.

For Strep●Tag pulldown assays, the RBM6Δ6 LVLQTM-derived peptide-coding sequence was cloned in frame between two BsaI sites within the pET-SUMO vector (Invitrogen), allowing its expression in fusion with the C terminus of the SUMO protein. In addition, the Strep●Tag sequence WSHPQFEK was added at the N terminus of the fusion protein. This construct was transferred into the pSCodon1 vector, and recombinant Strep●Tag-SUMO-LVLQTM was expressed in the *E. coli* SE1 strain. Subsequent incubation reactions were performed under the same conditions described above, except that equal volumes of cleared lysates prepared from bacteria overproducing either Strep●Tag-SUMO-LVLQTM or HRV-2 $2A^{pro}$–$(His)_6$ proteins were mixed (to a 1-ml final volume) with Strep-Tactin magnetic beads (Qiagen). Proteins which were specifically bound to the washed beads were separated by 15% SDS-PAGE and visualized by staining with Coomassie brilliant blue R250. $(His)_6$-tagged proteins were also revealed with a polyclonal antihistidine antibody (Cell Signaling).

Cleavage of TRPIITTA–pNA substrate by HRV-2 $2A^{pro}$. Cleavage of the TRPIITTA–*p*-nitroanilide (pNA) substrate by HRV-2 $2A^{pro}$ was performed at 25°C for 10 min in a 1-ml reaction mix containing 50 mM HEPES-NaOH, pH 8.0, 100 mM NaCl, 1 mM EDTA, 10 mM DTT, and purified recombinant HRV-2 $2A^{pro}$ (0.2 μM). The reaction was started by the addition of the TRPIITTA-pNA peptide (Eurogentec) at 25 μM and monitored continuously at 405 nm to characterize the initial velocity of the cleavage reaction. Peptide competition cleavage assays were performed under the same conditions, except that purified Strep●Tag-SUMO-LVLQTM protein (0 to 25 μM) was added to the reaction mix. Percent inhibition values were referred to as the ratio between initial velocity cleavage values measured with and without inhibitor. Data are expressed as means of three independent experiments, and standard deviations are indicated.

Molecular modeling. The crystal structure of the free HRV-2 $2A^{pro}$ has been used (Protein Data Bank [PDB] accession number 2hrv) (24). The conformation of the LVLQTM peptide was modeled using the one in complex with the foot-and-mouth disease virus (FMDV) $3C^{pro}$ as a starting model (PDB accession number 2wv4) (35). Side chains from the FMDV 3C protease-bound peptide were replaced with the side chains of VLQTM and then energy minimized using a GROMOS96 43B1 force field (32).

Cell culture and transient expression. Human epithelial lung carcinoma A549 cells (CCL-185; ATCC) were grown in Dulbecco's modified Eagle's medium (DMEM; Lonza) and 1 g/liter glucose supplemented with 10% fetal calf serum, 2 mM L-glutamine, penicillin, and streptomycin. $RBM6\Delta6_{274\text{-}520}$- and $RBM6\Delta6_{274\text{-}514}$-coding sequences were amplified by PCR and cloned into the multiple-cloning site of the pCI-neo vector (Promega) downstream from the following 2× Strep●Tag sequence: MASWSHPQFEKGGGSGGGSGGGSWSHPQFEK (where the underlining indi-

cates the Strep●Tag sequence). All plasmid constructs were transfected into cells using NanoJuice transfection reagents (Novagen), according to the manufacturer's instructions.

Western blotting. Proteins were separated by SDS-PAGE and transferred onto nitrocellulose membranes. The membranes were incubated for 1 h in Tris-buffered saline containing 0.1% Tween 20 and 5% nonfat milk powder at room temperature. Membranes were then incubated overnight at 4°C with a polyclonal antihistidine antibody (reference no. 2365; Cell Signaling) or an antiserum recognizing the C-terminal domain of eIF4G (19). These antibodies were revealed using the horseradish peroxidase-coupled goat antirabbit antibody, followed by chemiluminescence detection using the SuperSignal West Pico chemiluminescent substrate from Pierce.

***In vitro* transcription and RNA transfection.** Plasmids containing the 2A protease-coding region were constructed by inserting the respective coding sequences into the pGlobin-*Renilla* vector (29). For *in vitro* transcription, DNA templates were linearized at the EcoRI site downstream from a synthetic poly(A) tail. Capped RNAs were transcribed using the T7 RNA polymerase as previously described (25) and treated with RQ1 DNase (Promega). The integrity of the RNAs was checked by electrophoresis on nondenaturing agarose gels, and the concentration was quantified by spectrophotometry at 260 nm using a Nanodrop apparatus (Nanodrop Technologies).

Two days before RNA transfection, A549 cells were seeded into 48-well plates at 75,000 cells per well to reach about 180,000 cells at the time of transfection. RNA transfection was performed with 100 ng of $2A^{pro}$-coding RNA and the TransIT kit (Mirus Bio) for 2 h and 50 ng of *Renilla*-coding RNA for additional 3 h. The cells were then harvested, and luciferase activity was quantified using the *Renilla* luciferase (R-Luc) assay system from Promega and a Veritas microplate luminometer (Turner BioSystems). Transfection efficiency was evaluated by transfecting the green fluorescent protein (GFP)-coding RNA under the same conditions and counting the number of green fluorescent cells by fluorescence-activated cell sorter (FACS) analysis. Over 70% of A549 cells expressed GFP.

Virus infection. HRV-2 (GenBank accession number X02316) and HRV-14 (GenBank accession number K02121) were provided by the WHO/National Reference Centre for Enteroviruses (Lyon, France). A549 cells (90% confluence) were infected with HRV-2 or HRV-14 at a multiplicity of infection (MOI) of 1 in DMEM containing 2% fetal calf serum, 2 mM L-glutamine, penicillin, and streptomycin and incubated at 34°C. Virus titer was quantified by the 50% tissue culture infectious dose ($TCID_{50}$) assay using MRC5 cells according to the method of Reed and Muench (26).

Infection and mouse treatment. Six-week-old BALB/c female mice were purchased from Charles River Laboratories, and experiments were undertaken as previously described (13). On the day of infection, a three-step protocol was used for peptide administration: (i) first, mice were anesthetized by intraperitoneal injection of ketamine (42.5 mg/kg of body weight), (ii) then, a 25-μl volume of HRV-2 suspension containing 100,000 PFU was injected dropwise to the external nares of the mice using a micropipette, and (iii) finally, a 25-μl volume of the indicated concentration of peptide solution dissolved in 1% dimethyl sulfoxide (DMSO) was administered in the same way either right after infection or at 12 h postinoculation. Lungs were harvested at different time points postinfection and ground in the Tissue Lyser LT device from Qiagen. After centrifugation at 12,000 × *g* for 5 min at 4°C, supernatants were collected and virus titers were determined as described above. Ten mice were used for each experimental condition.

Statistical analysis. The Mann-Whitney U test was used to evaluate statistical significance ($P < 0.05$) of viral replication *in vivo*.

RESULTS

Yeast two-hybrid screening for proteins interacting with HRV-2 $2A^{pro}$. In order to identify partners and potential inhibitors of HRV $2A^{pro}$, a plasmid expressing a LexA–HRV-2 $2A^{pro}$ fusion protein was used to screen a human placenta cDNA library using Y187 (*mat*α) and L40αGal4 (*mat***a**) yeast strains. Fifty million clones were screened, and 51 His^+ colonies were further isolated and characterized by DNA sequencing and sequence alignment analysis. Among these clones, nine encoded out-of-frame short polypeptides and one encoded the C-terminal part (amino acids 274 to 520) of the functionally uncharacterized RBM6Δ6 protein (GenBank accession number FLJ56542) (31). As depicted in Fig. 1, all exhibited related sequences that shared the same peptide consensus motif LXLX(T/N)Φ, where X represents any amino acid and Φ represents a hydrophobic residue. Interestingly, this sequence partially mimics the consensus sequence $_{P4}LX(T/N)X_{P1}$ found in $2A^{pro}$ substrates where threonine (or asparagine) and leucine are required in positions P2 and P4, respectively, for $2A^{pro}$ cleavage (16). In addition, the tripeptide motifs $_{P3}QTM_{P1}$ and $_{P4}LQT_{P2}$ found in the RBM6Δ6 sequence are identical to those found at the corresponding positions within the $2A^{pro}$ substrates PABP1 and VP1-$2A^{pro}$ junction of the HRV-62 polyprotein, respectively (16). Finally, the presence of methionine at the P1 position represents a favorable determinant for $2A^{pro}$ binding (28). Remarkably, the presence of a conserved leucine (or an equivalent hydrophobic residue) at the P6 position in all selected peptides suggests that this amino acid may represent an important parameter in the specificity of recognition by $2A^{pro}$. Thus, these results strongly suggested that the LXLX(T/N)Φ motif peptides isolated in the double-hybrid screening are partners of HRV-2 $2A^{pro}$.

CL27/	TVSTYIHIQQTQVDFYAGKSEMPVCR	L	R	L	K	N	$L_{(COOH)}$
CL35/	PNGFRPFCCHTQQTMGWAFRPSQGHQG	L	R	L	R	N	$L_{(COOH)}$
CL45/	LRLHACKVK	I	K	L	V	T	$L_{(COOH)}$
CL52/	GRKQS	L	S	L	V	T	$L_{(COOH)}$
CL41/	DPL	F	R	L	T	T	$L_{(COOH)}$
CL22/	ARARCHRGRGEGSSSVRKAATLPQDGT	L	C	L	H	T	$C_{(COOH)}$
CL51/	GIN	L	F	L	Y	T	$C_{(COOH)}$
CL25/	FAYLFKNKKNTQNKFK	L	Y	I	Y	T	$V_{(COOH)}$
CL43/	ARSWT	L	K	L	Q	T	$V_{(COOH)}$
CL46/	RBM6Δ6(aa 274-514)	L	V	L	Q	T	$M_{(COOH)}$
	Consensus sequence	**L**	**X**	**L**	**X**	**T/N**	**Φ**

	Cleavage site	P_6	P_5	P_4	P_3	P_2	P_1/P'_1
HRV-2 polyprotein		R	I	I	T	T	A/GPS
HRV-62 polyprotein		Q	N	L	Q	T	A/GPS
PABP		T	S	T	Q	T	M/GPR

FIG 1 Amino acid sequences of the HRV-2 $2A^{pro}$-binding peptides identified by the yeast two-hybrid system. Peptides are arranged to illustrate the consensus sequence found, where X is any amino acid and Φ is a hydrophobic amino acid. Alignments of the carboxy termini of $2A^{pro}$-binding peptides with natural cleavage sites of $2A^{pro}$ are also shown.

The LXLX(T/N)Φ motif behaves as a pseudosubstrate of HRV-2 $2A^{pro}$. To investigate whether the previously characterized peptides were pseudosubstrates of HRV-2 $2A^{pro}$, different hybrid peptides were built by fusing the six terminal amino acid residues of the 10 polypeptides identified by yeast two-hybrid screening with the GPSDM sequence found at the P1′ and P5′ positions of the authentic *cis*-cleavage site of the HRV-2 polyprotein (Fig. 1). The 11-mer peptides obtained were then inserted in frame into a genetically engineered firefly luciferase which was synthesized in a cell-free protein expression system in the presence of [^{35}S]methionine and used as a protease substrate (Fig. 2A). In this assay, cleav-

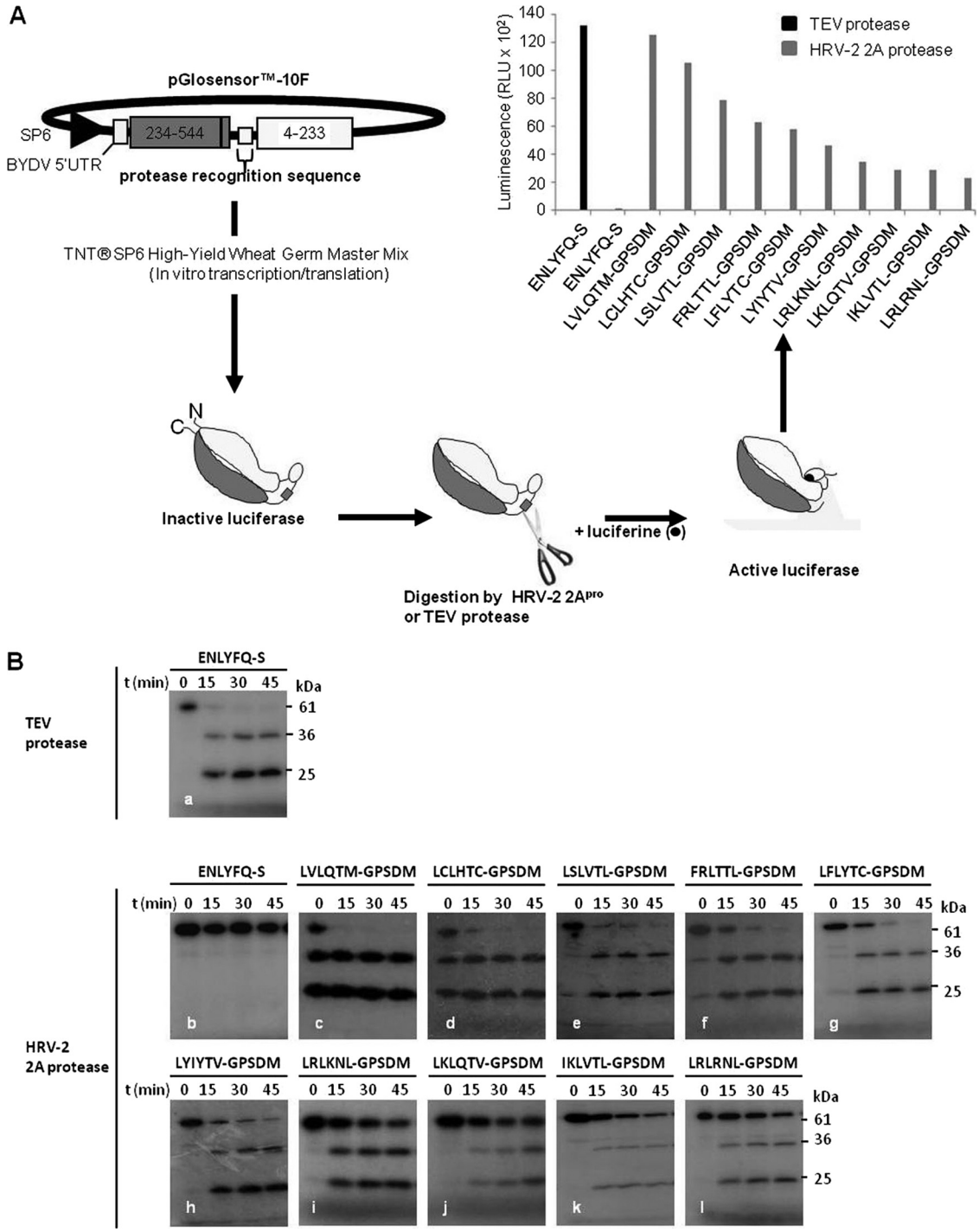

FIG 2 HRV-2 2A^{pro}-binding peptides identified by the yeast two-hybrid system are pseudosubstrates of the protease. (A) ^{35}S-labeled GloSensor protease site luciferase activation by HRV-2 2A^{pro} digestion of hybrid sites generated from sequences depicted in Fig. 1. To generate the GloSensor protein, new N and C termini were created at amino acids 234 and 233, respectively. The protein-coding region of this circularly permuted firefly luciferase was carried on the pGloSensor-10F linear vector. Insertion of a protease recognition sequence between these native N and C termini and cleavage of the sequence by the cognate protease activate the luciferase enzyme. Plasmid DNAs encoding the protease recognition sequences indicated on the graph were transcribed and translated *in vitro* and incubated with purified HRV-2 2A^{pro} or TEV protease for 45 min. Luminescent signal was measured by mixing an aliquot of each TNT reaction mixture with Bright-Glo assay reagent in triplicate and incubating for 5 min at room temperature. Luminescence was measured using a luminometer. A plasmid DNA encoding the ^{35}S-labeled GloSensor ENLYFQ-S protein, where ENLYFQ-S is a cleavage site of the TEV protease, was used as a control. RLU, relative light units. (B) The different ^{35}S-labeled GloSensor proteins containing the protease sites to be tested were synthesized *in vitro* as described above and then incubated with 2 μg of TEV protease or HRV-2 2A^{pro} for 45 min, followed by SDS-PAGE and fluorography. Gel patterns corresponding to enzymatic digestion performed with TEV protease (a) and HRV-2 2A^{pro} (b to l) are shown. The 0-h time point shows proteins that were harvested right after addition of the proteases in the incubation mixtures.

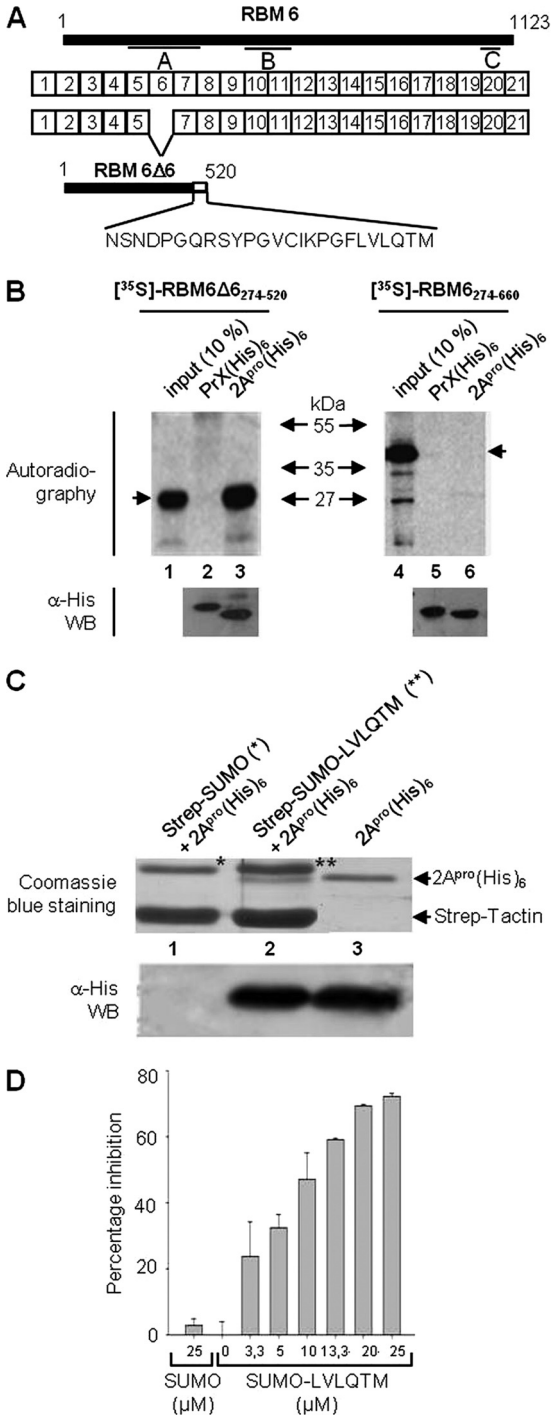

FIG 3 The last six residues of RBM6Δ6 are necessary and sufficient for the interaction with HRV-2 2A^{pro}. (A) Schematic representation of the exon structure of the *RBM6* gene and the protein products derived from two splice variants (data are from references 14 and 31). Boxes represent exons and are not drawn to scale. The bars below RBM6 indicate different protein motifs, as follows: A and B, RNA binding motif RNP1 and RNP2; C, G patch. In the truncated RBM6Δ6 protein, the amino acid residues represented by the white part differ from those in the longer protein product RBM6 due to a frame shift caused by the splicing. (B) Results of a His pulldown assay with HRV-2 2A^{pro} and RBM6Δ6. HRV-2 2A^{pro}–$(His)_6$ was immobilized on affinity resin and incubated with *in vitro*-translated ^{35}S-labeled RBM6Δ$6_{274\text{-}520}$ or RBM$6_{274\text{-}660}$ protein. Bound proteins were resolved by SDS-PAGE and visualized by autoradiography. Lanes 1 and 4, 10% of total proteins from the initial incubation reaction; lanes 2 and 3, incubation of ^{35}S-labeled RBM6Δ$6_{274\text{-}520}$ with a control His-tagged protein and HRV-2 2A^{pro}–$(His)_6$, respectively; lanes 5 and 6, the corresponding assays conducted in the presence of RBM$6_{274\text{-}660}$. Binding of His-tagged proteins on the affinity resin was checked by Western blotting (WB) using an antihistidine antibody. (C) Results of a Strep●Tag pulldown assay with HRV-2 2A^{pro} and the RBM6Δ6-derived LVLQTM sequence. Bacterially expressed Strep●Tag-SUMO or Strep●Tag-SUMO-LVLQTM was incubated with HRV-2 2A^{pro}–$(His)_6$ and Strep-Tactin-coated magnetic beads. A Coomassie blue-stained gel of proteins bound on the affinity resin is presented: lane 1, Strep●Tag-SUMO and HRV-2 2A^{pro}–$(His)_6$; lane 2, Strep●Tag-SUMO-LVLQTM and HRV-2 2A^{pro}–$(His)_6$; lane 3, purified HRV-2 2A^{pro}–$(His)_6$. Symbols: *, Strep●Tag-SUMO; **, Strep●Tag-SUMO-LVLQTM. The presence of HRV-2 2A^{pro}–$(His)_6$ was confirmed by Western blot analysis using an antihistidine antibody. (D) Effect of the RBM6Δ6-derived peptide LV LQTM on cleavage of TRPIITTA–*p*-nitroanilide (TRPIITTA-pNA) by HRV-2 2A^{pro}. Various concentrations of the purified SUMO-LVLQTM protein (0 to 25 μM) were added to the TRPIITTA-pNA peptide, and their inhibitory effect on HRV-2 2A^{pro} catalysis was measured by collecting absorbance at 405 nm for 10 min at 25°C. The percentage of cleavage activity was calculated relative to the value obtained with no inhibitor. Data are expressed as means of three independent experiments, and standard deviations are indicated. SUMO protein was used as a control.

age of the recombinant luciferase at the protease recognition sequence led to the activation of the luciferase enzyme, resulting in an increase in luminescence when a firefly luciferase substrate was added to the reaction mixture. Thus, if a peptide acted as a pseudosubstrate for 2A^{pro}, an increase in luciferase activity would be observed. As shown in Fig. 2A, significant luciferase activity was detected for all constructs tested, and the best score was measured for the ^{35}S-labeled GloSensor LVLQTM-GPSDM protein, the protease site of which was derived from the C terminus of the RBM6Δ6 protein. Luminescence was hardly detectable when using the negative control, ^{35}S-labeled GloSensor-10F ENLYFQ-S protein, which was recognized by the tobacco etch virus protease but not by HRV-2 2A^{pro}. In contrast and as expected, the ^{35}S-labeled GloSensor-10FENLYFQ-S protein was cleaved by the TEV protease, resulting in increased luminescence. Thus, our results confirmed that all peptides isolated by yeast two-hybrid screening behaved as potent substrate analogues of HRV-2 2A^{pro}.

Cleavage of the ^{35}S-labeled GloSensor-10F-identified peptide-GPSDM luciferases (61 kDa) by HRV-2 2A^{pro} was also visualized after separation of digested products by SDS-PAGE and autoradiography (Fig. 2B, panels c to l). Total inactivation of the proteases was effective only by boiling the sample for 5 min in SDS loading buffer, which may explain the partial substrate degradation at the initial time in panels c and d and reflected a higher affinity of HRV-2 2A^{pro} for LVLQTM-GPSDM and LCLHTC-GPSDM sequences than for the other substrates. Moreover, all ^{35}S-labeled GloSensor-10F-identified peptide-GPSDM luciferases were hydrolyzed by HRV-2 2A^{pro} into two predictive fragments of 36 and 25 kDa, confirming that all identified peptides were substrate analogues of 2A^{pro}. As expected, the ^{35}S-labeled GloSensor-10F ENLYFQ-S protein was cleaved by the TEV protease but not by the 2A protease of HRV-2 (Fig. 2B, compare panels a and b). In addition, the kinetics of digestion were peptide dependent, with the highest rate being for the LVLQTM peptide. Thus, these results confirmed that the identified peptides acted as pseudosubstrates for HRV-2 2A^{pro}.

The LVLQTM peptide specifically interacts with HRV-2 2A^{pro}. Since the LVLQTM peptide displayed the highest affinity for the 2A protease, the interaction between these two binding

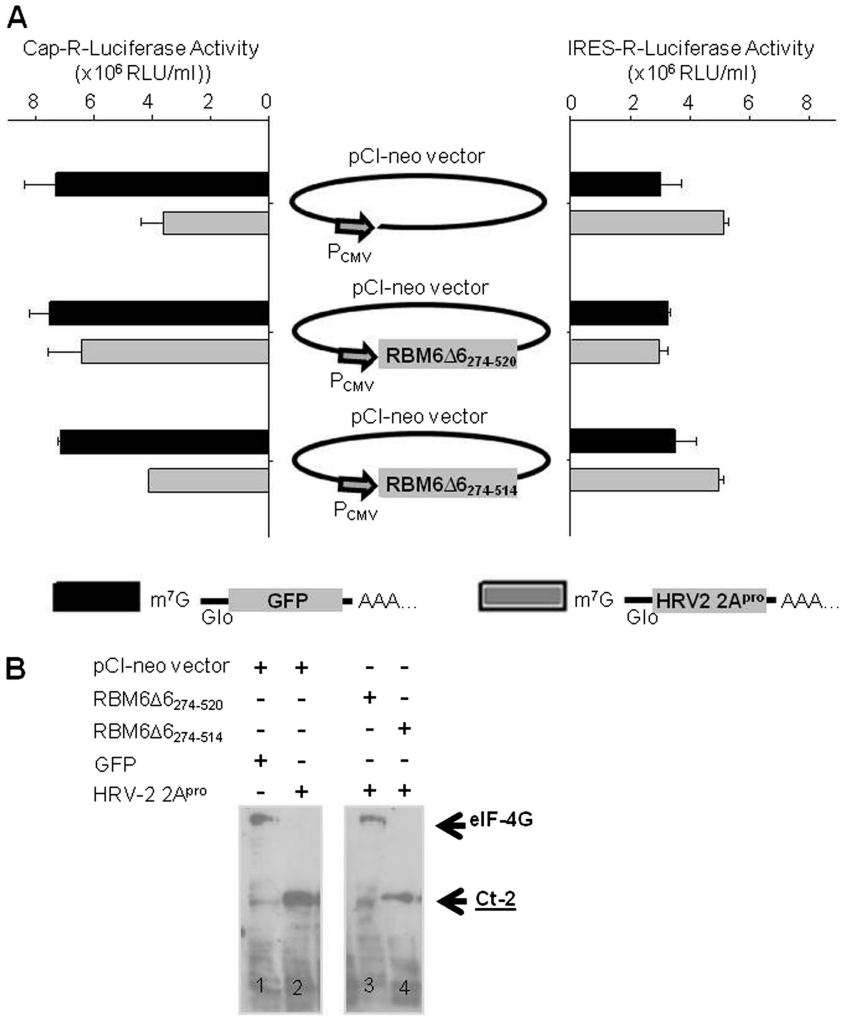

FIG 4 RBM6Δ$6_{274\text{-}520}$ inhibits eIF4G cleavage activity of HRV-2 $2A^{pro}$ in A549 cells. (A) A549 cells were transfected for 24 h with a pCI-neo plasmid harboring either the *RBM6*Δ$6_{274\text{-}520}$ or the *RBM6*Δ$6_{274\text{-}514}$ gene under the control of the cytomegalovirus (CMV) promoter and were subsequently transfected with an mRNA coding for HRV-2 $2A^{pro}$ or GFP for 2 h. The effect of the 2A protease on eIF4G cleavage and thus on the translation of capped mRNA was measured using a capped mRNA or an IRES-containing mRNA, both coding for the *Renilla* luciferase. The first contained the 5′ UTR of the β-globin gene, which directed cap-dependent translation. The second contained the 5′ UTR of the encephalomyocarditis virus (EMCV) RNA, which ensured an IRES-dependent translation. After 3 h of transfection of the luciferase RNAs, cells were lysed and luciferase activity was measured by luminometry. Error bars denote the standard deviation from the mean of three independent experiments. (B) Inhibition of the eIF4G cleavage activity of HRV-2 $2A^{pro}$. A549 cells transiently expressing 2× Strep●Tag–RBM6Δ$6_{274\text{-}520}$ protein or 2× Strep●Tag–RBM6Δ$6_{274\text{-}514}$ for 24 h were subsequently transfected with an mRNA coding for HRV-2 $2A^{pro}$ or the GFP for 5 h. Total protein extracts (60 μg) were prepared from transfected cells, separated by 6% SDS-PAGE, and blotted with an antibody directed against the C-terminal part of the eIF4G protein. The main cleavage product (at about 100 kDa) which resulted from the proteolytic activity of $2A^{pro}$ is indicated Ct-2. The pCI-neo vector was used as a control for plasmid transfection. Of note, cells were lysed in the absence of protease inhibitor cocktail, possibly explaining the partial eIF4G hydrolysis observed in lanes 1 and 3.

partners was analyzed by two complementary pulldown assays. First, *in vitro*-translated [^{35}S]methionine-labeled RBM6Δ$6_{274\text{-}520}$ (truncated protein detected by yeast two-hybrid screening, 28 kDa) or its alternative splicing isoform, $RBM6_{274\text{-}660}$ (44 kDa, Fig. 3A), was incubated with purified recombinant HRV-2 $2A^{pro}$–$(His)_6$ or with a His-tagged control protein bound to Ni-NTA magnetic agarose beads. As measured by densitometric analysis, about 15% of total RBM6Δ$6_{274\text{-}520}$ input bound to immobilized HRV-2 $2A^{pro}$ (Fig. 3B; compare lanes 1 and 3) but not to the control His-tagged protein (lane 2). In contrast, $RBM6_{274\text{-}660}$ failed to bind either protein (lanes 5 and 6). These results demonstrated that RBM6Δ$6_{274\text{-}520}$ specifically interacted with HRV-2 $2A^{pro}$. Since RBM6Δ$6_{274\text{-}520}$ differed from $RBM6_{274\text{-}660}$ by its last 25 residues (Fig. 3A) and this region contained the particular LV LQTM sequence that was previously identified in the yeast two-hybrid system, these results suggested that LVLQTM was directly involved in the interaction with $2A^{pro}$.

A Strep●Tag pulldown assay was then used to investigate whether LVLQTM-derived peptide was sufficient for $2A^{pro}$ binding (Fig. 3C). To this end, LVLQTM was first expressed in bacteria in fusion to the C terminus of a Strep●Tag-SUMO protein that allowed high specific binding on a Strep-Tactin affinity resin. Bacterial cell lysates containing either the Strep●Tag-SUMO-LV LQTM or the control Strep●Tag-SUMO recombinant protein were then mixed with a crude bacterial extract enriched with the recombinant HRV-2 $2A^{pro}$–$(His)_6$ protein. After 1 h of incubation

with the Strep-Tactin resin, protein complexes were subjected to SDS-PAGE separation and Coomassie blue staining or Western blotting using an antihistidine antibody (Fig. 3C). Results revealed that HRV-2 2A^{pro}–$(His)_6$ proteins coeluted with Strep●Tag-SUMO-LVLQTM protein (lane 2) but not with Strep●Tag-SUMO protein (lane 1). Therefore, the LVLQTM peptide was necessary and sufficient for the interaction with 2A^{pro}. Altogether, these results identified LVLQTM as a binding partner of HRV-2 2A^{pro}.

HRV 2A^{pro} activity is inhibited by LVLQTM in a strain-independent manner. We next investigated whether LVLQTM binding to HRV-2 2A^{pro} inhibited its activity. To this end, the 2A^{pro} activity was measured *in vitro* by a specific cleavage assay using the chromogenic substrate TRPIITTA–*p*-nitroanilide, which mimics the native HRV-2 2A^{pro} substrate sequence at the VP1-2A junction. As shown in Fig. 3D, addition of increasing concentrations of the Strep●Tag-SUMO-LVLQTM protein inhibited the activity of 2A^{pro} in a dose-dependent manner. The residual enzyme activity was about 30% at a saturating concentration of inhibitor (25 μM). Control experiments showed that at the same concentration, the Strep●Tag-SUMO protein did not display any inhibitory effect on protease activity. Thus, LVLQTM inhibited the activity of the viral enzyme *in vitro*.

To investigate whether inhibition of 2A^{pro} by LVLQTM was relevant *in cellulo*, a three-step procedure for quantifying the inhibitory effect of LVLQTM on the cleavage of eIF4G by HRV-2 2A^{pro} was designed. In this protocol, A549 cells were transfected (i) for 24 h with a plasmid expressing either the RBM6$\Delta 6_{274\text{-}520}$ fragment or the RBM6$\Delta 6_{274\text{-}514}$ fragment which was deleted from the LVLQTM motif, then (ii) for 2 h with a capped and polyadenylated mRNA coding for the HRV-2 2A^{pro} or the GFP protein as a control, and finally (iii) for 3 h with a reporter *Renilla* luciferase (R-Luc) mRNA containing either the 5′ untranslated (UTR) of the β-globin gene (capped mRNA) or the encephalomyocarditis virus (EMCV) internal ribosome entry site (IRES) sequence (uncapped mRNA). This assay relied on the fact that in eukaryotic cells, the distribution of mRNAs between capped and uncapped is largely in favor of capped mRNAs, for which translation initiation depends on intact initiation complex factors eIF4G/eIF4E. In contrast, translation of IRES-containing RNAs can occur in the presence of proteolyzed eIF4G, as the latter requires only the carboxy-terminal part of the eIF4G molecule. Thus, the presence of intact eIF4G allows the translation of capped mRNAs and its hydrolysis indirectly benefits the translation of uncapped mRNA. As depicted in Fig. 4, in the presence of the pCI-neo vector (empty vector) and the GFP-coding RNA, eIF4G was not cleaved (Fig. 4B, lane 1) and translation of capped mRNA, as measured by reporter Cap–R-Luc, activity was favored compared to IRES-driven translation, which explained the low level of IRES–R-Luc activity (Fig. 4A). In contrast, expression of HRV-2 2A^{pro} in the presence of the pCI-neo empty vector led to eIF4G cleavage (Fig. 4B, lane 2), which inhibited capped mRNA translation and indirectly increased IRES-driven translation, as measured by the decrease in Cap–R-Luc activity and the increase in IRES–R-Luc reporter activity (Fig. 4A). In cells overproducing the authentic C terminus of the RBM6Δ6 protein (RBM6$\Delta 6_{274\text{-}520}$), the eIF4G cleavage activity of 2A^{pro} was notably reduced (Fig. 4B, lane 3) and the level of Cap-dependent luciferase translation was mildly affected (Fig. 4A). Expression of the C terminus of the RBM6Δ6 protein deleted from the LVLQTM sequence (RBM6$\Delta 6_{274\text{-}514}$) did not affect

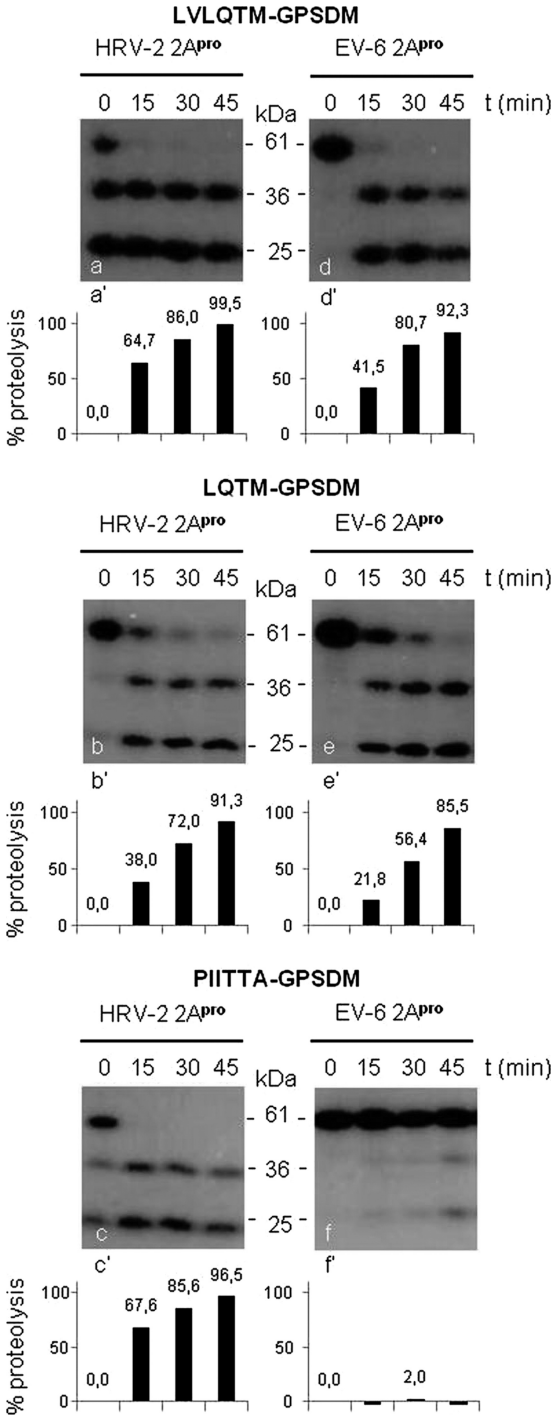

FIG 5 The RBM6Δ6-derived LVLQTM peptide is a pseudosubstrate of HRV-2 and EV-6 2A^{pro}. Three different ^{35}S-labeled GloSensor proteins containing the protease sites to be tested were synthesized *in vitro* under the same conditions described in the legend of Fig. 2 and then incubated with 2 μg of HRV-2 2A^{pro} or EV-6 2A^{pro} for 45 min in cleavage buffer, followed by SDS-PAGE and fluorography. Gel patterns corresponding to enzymatic digestion performed with HRV-2 2A^{pro} (a to c) or EV-6 2A^{pro} (d to f) are shown. The percent hydrolysis of the ^{35}S-labeled GloSensor luciferases was determined by densitometric analysis of the 61-kDa band and calculated relative to its initial (0-min) intensity (a′ to f′). The 0-h time point shows proteins that were harvested right after addition of the proteases in the incubation mixtures.

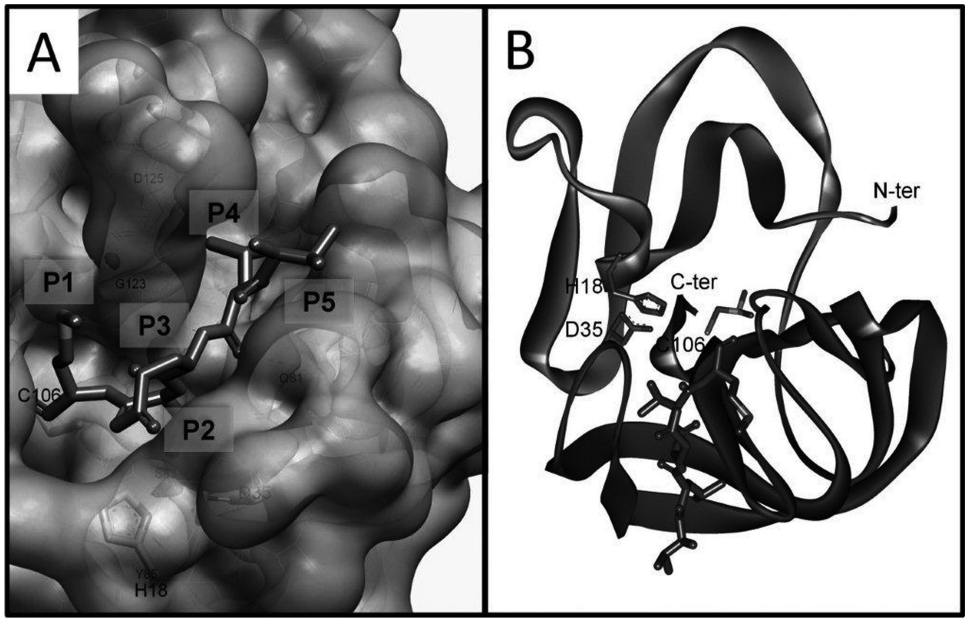

FIG 6 Model of the interaction between VLQTM peptide and substrate-binding pocket residues of HRV-2 2A^{pro}. (A) Close-up view of the binding of the P5 to P1 residues from the LVLQTM inhibitor. The protease backbone is depicted as a line covered by a semitransparent Van der Walls surface, except for catalytic residues with large labels, depicted as sticks; protease-interacting residues have small labels. (B) Ribbon diagram of the overall structure of HRV-2 2A^{pro} in complex with the peptidic inhibitor. Catalytic triad residues are labeled. C-ter, C terminus; N-ter, N terminus.

HRV-2 2A^{pro} activity, showing that the RBM6$\Delta 6_{274\text{-}520}$ fragment specifically inhibited HRV-2 2A^{pro} activity through its LVLQTM motif.

We further investigated whether LVLQTM binding to 2A^{pro} was strain specific. To this end, susceptibility of the ^{35}S-labeled GloSensor LVLQTM-GPSDM protein to degradation by the HRV-2 2A protease was compared to that by the echovirus 6 (EV-6) 2A^{pro} by the protease-Glo assay described above. Briefly, after *in vitro* translation with [^{35}S]methionine, the recombinant luciferase was incubated with purified HRV-2 2A^{pro} or EV-6 2A^{pro}, and the resulting digestion products were then separated by SDS-PAGE and visualized by autoradiography after treatment of gels with a fluorography solution. As shown in Fig. 5a, cleavage of full-length luciferase into its 36-kDa and 25-kDa predicted fragments was almost complete when HRV-2 2A^{pro} was added to the reaction mix (0 h). Interestingly, a sequence lacking the LV residues (LQTM-GPSDM; Fig. 5b) had a significantly reduced hydrolysis rate (38%; Fig. 5b′) after a 15-min incubation with the HRV-2 2A protease, showing that deletion of P5 and P6 residues in the LVLQTM-GPSDM sequence was detrimental to the recognition by HRV-2 2A^{pro}. A control luciferase containing the authentic cleavage site found in the HRV-2 polyprotein (PIITTA-GPSDM; Fig. 5c and c′) was cut by HRV-2 2A^{pro} to the same extent as the LVLQTM-GPSDM hybrid site (Fig. 5a and a′). Similar results were obtained when reactions were carried out in the presence of purified 2A^{pro} enzyme from EV-6, another member of the enterovirus genus (compare Fig. 5a to d and b to e, respectively). In contrast, a marked difference was observed for the HRV-2 control site, PIITTA-GPSDM, which, while cut by HRV-2 2A^{pro}, was hardly recognized by the EV-6 2A^{pro} (compare Fig. 5c and f), thus reflecting differences in substrate specificity between the two proteases, which share a relatively low level (40%) of amino acid sequence identity. Finally, the LVLQTM sequence in RBM6Δ6 seemed to bind to the substrate-binding pocket of both HRV-2 and EV-6 2A^{pro}, thus suggesting that this peptide may be effectively recognized by and thereby inhibit a wide range of 2A proteases.

Virtual docking of LVLQTM peptide into HRV-2 2A^{pro} catalytic site. To get further insights into the interaction between the protease and its peptidic inhibitor, we decided to explore the orientations of the peptide by virtual docking in the substrate-binding pocket of HRV-2 2A^{pro}. In conjunction, an extensive investigation of the impact of sequence variation in the peptide on the rate of cleavage was performed.

In the model depicted in Fig. 6B, the peptide largely bound within a deep surface groove that was diagonally oriented and intersected the cleft at the active site. Consequently, residues P5 to P1 mainly contacted the C-terminal β barrel, and the length of the groove was sufficient to accommodate residues P4 to P1 of the peptide. P5 Val at the N terminus of the peptide was largely solvent exposed (Fig. 6A), making a unique H bond through its N terminus, while its side chain was surrounded by polar side chains of Gln81 and Asp125. This lack of specific contact might suggest only a modest effect on substrate cleavage upon substitution at this position. On the other hand, P4 Leu was accommodated in an apolar depression defining the beginning of the peptide-binding groove, which consisted of side chains of Tyr78, Ile80, Ile96, and Ala129 (Fig. 6A). The side chain of P3 Gln pointed toward the solvent, which explained why, in common with other similar proteases, there was no strong preference for a particular residue at this position. Indeed, as shown by the protease-Glo assay approach, peptides displaying relatively different residues (Q, H, or V) at the P3 position were digested to about the same extent by 2A^{pro} (Fig. 2A and B). The P2 Thr side chain inserted into the cleft between the β barrel and the N-terminal β sheet of the protease (Fig.

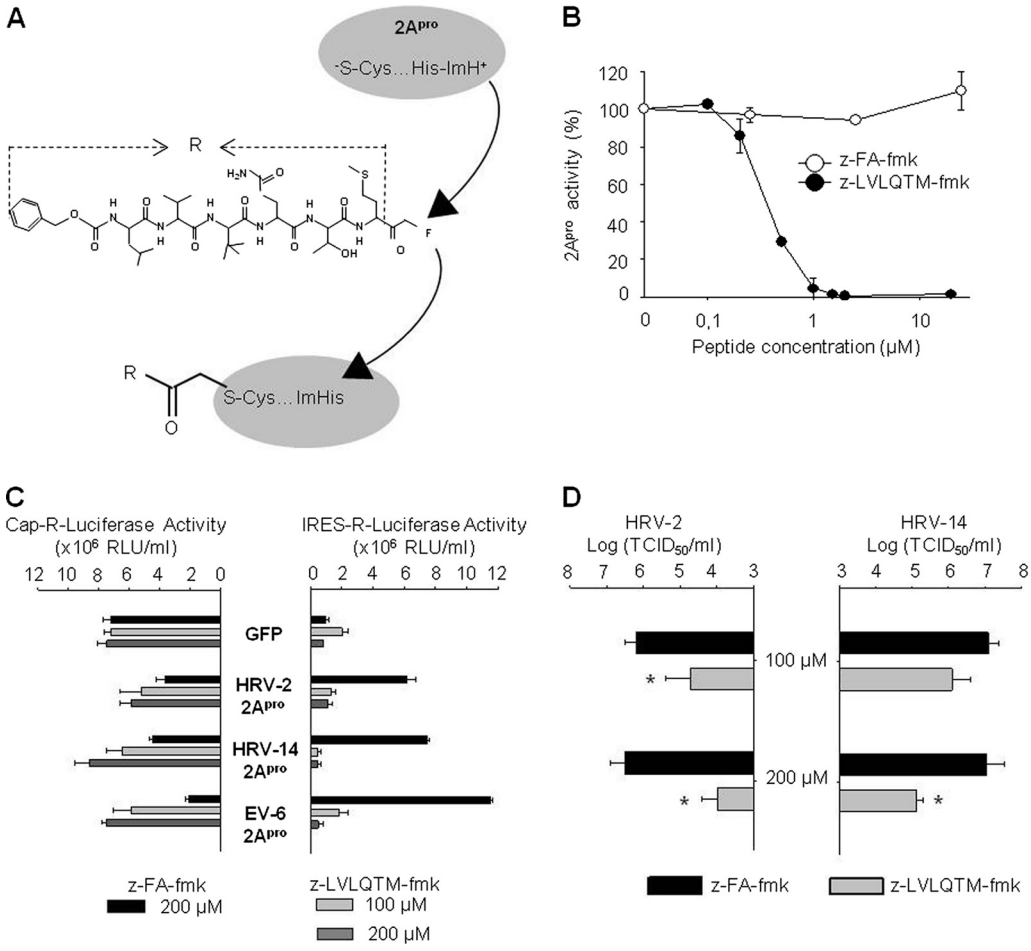

FIG 7 The z-LVLQTM-fmk peptide inhibits 2A^{pro} activity and HRV replication in A549 cells. (A) The LVLQTM peptide was synthesized and modified (MP Biomedicals Company) by adding a benzyloxycarbonyl (z) at its N terminus and a fluoromethylketone (fmk) group at its C terminus to form z-LVLQTM-fmk. The latter is known to form a covalent link with the catalytic cysteine of the 2A^{pro} (20). (B) Effect of z-LVLQTM-fmk on cleavage *in vitro* of TRPIITTA–*p*-nitroanilide by the HRV-2 2A^{pro}. Various concentrations (0 to 25 μM) of z-LVLQTM-fmk or z-FA-fmk (RnD Systems) were added to the TRPIITTA-pNA peptide, and their effects on HRV-2 2A^{pro} catalysis was measured by collecting the absorbance at 405 nm for 10 min at 25°C. The percentage of cleavage activity was calculated relative to the value obtained with no inhibitor. Data are expressed as means of three independent experiments, and standard deviations are indicated. (C) A549 cells were treated with 100 μM or 200 μM z-LVLQTM-fmk or z-FA-fmk for 1 h and were subsequently transfected with an mRNA coding for HRV-2 2A^{pro}, HRV-14 2A^{pro}, EV-6 2A^{pro}, or GFP for 2 h. Cells were then transfected for 3 h with a capped mRNA or an IRES-containing mRNA, both coding for the *Renilla* luciferase. The first contained the 5′ UTR of the β-globin gene, and the second contained the 5′ UTR of the encephalomyocarditis virus (EMCV) RNA. Cells were subsequently lysed, and luciferase activity was measured by luminometry. Error bars denote the standard deviations from the mean values obtained from three independent experiments. (D) A549 cells were treated with different concentrations of z-LVLQTM-fmk or z-FA-fmk and infected with HRV-2 or HRV-14 at a multiplicity of infection of 1 for 12 h. The $TCID_{50}$ in the supernatant of infected cells was determined as described in Materials and Methods.

6A), where it made two hydrogen bonds with residues Ser83 and Tyr85, both belonging to the same side of the pocket. In our model and contrary to the one discussed by Petersen et al. (24), binding of P2 Thr did not require a prior rotation of Tyr85.

Finally, the P1 Met side chain made three hydrogen bonds with the substrate-binding pocket: two between its carbonyl group and both the carbonyl and side chain of Cys106 (3.1 Å for both H bonds) and one between its N atom and the hydroxyl group of Tyr85 (2.9 Å) (Fig. 6A). The flat and narrow pocket displayed very good chemical complementarities to the P1 Met side chain.

In the light of this structural model, we showed that the double mutation S83A/D125A resulted in an approximately 20-fold decrease in the initial rate of TRPIITTA-pNA hydrolysis by 2A^{pro} (data not shown), confirming that these two residues played a major role in the interaction with the LVLQTM peptide.

The z-LVLQTM-fmk peptide inhibits the replication of HRV-2 in A549 cells. As LVLQTM was found to inhibit 2A^{pro} activity, we then investigated whether it also inhibited HRV replication *ex vivo*. As pseudosubstrates are more potent inhibitors when covalently bound to their target proteases, we synthesized a modified LVLQTM peptide containing a fluoromethylketone group at its C terminus which forms a persistent, nonlabile covalent bond with the catalytic cysteine (Fig. 7A). Moreover, a benzyloxycarbonyl group was added at its N terminus to increase its cell permeation. As expected, the z-LVLQTM-fmk molecule gave a sharp decrease in HRV-2 2A^{pro} activity in the TRPIITTA–*p*-nitroanilide substrate cleavage assay with a 50% inhibitory con-

centration value of 0.3 μM (Fig. 7B). In contrast, no inhibitory effect on 2A^{pro} activity was observed when this assay was conducted in the presence of the control peptide z-FA-fmk, which shared the same chemical changes as z-LVLQTM-fmk. Furthermore, inhibition of capped mRNA translation by HRV-2 2A^{pro} was significantly reduced by the z-LVLQTM-fmk peptide used at 100 μM and 200 μM (Fig. 7C) compared to the z-FA-fmk control peptide. These concentrations showed no cytotoxic effect on A549 cells (data not shown). The same inhibitory effect was observed using the same test with HRV-14 2A^{pro} (belonging to the rhinovirus species B) and EV-6 2A^{pro}, which again reinforced the idea that z-LVLQTM-fmk was not strain specific (Fig. 7C). Thus, the z-LV LQTM-fmk-modified peptide strongly and specifically inhibited several 2A^{pro} enzymes.

We next investigated the effect of LVLQTM on virus replication in A549 cells. For this purpose, cells were infected with HRV-2 or HRV-14 at a multiplicity of infection (MOI) of 1 in the presence of z-LVLQTM-fmk (100 μM or 200 μM) or the unrelated control peptide z-FA-fmk. At 12 h postinfection, the 50% tissue culture infective dose ($TCID_{50}$) value in the supernatants of infected cells was determined. Results depicted in Fig. 7D indicated that the z-LVLQTM-fmk peptide inhibited HRV-2 and HRV-14 replication in a dose-dependent manner compared to the unrelated control peptide. Altogether, our data demonstrated that the observed decrease in virus production correlated directly with 2A^{pro}-mediated inhibition by the z-LVLQTM-fmk peptide.

The z-LVLQTM-fmk peptide protects against rhinovirus infection *in vivo*. To assess the role of z-LVLQTM-fmk *in vivo*, we investigated whether z-LVLQTM-fmk could inhibit HRV replication in mice. For this purpose, mice were inoculated with HRV-2 (10^5 PFU/mouse) and, at the same time, treated or not with various concentrations of z-LVLQTM-fmk. Lungs of infected mice were then harvested at different time points postinfection, and infectious particles were evaluated by determining the $TCID_{50}$. As shown in Fig. 8A, compared to DMSO-treated mice, z-LVLQTM-fmk-treated mice had significantly fewer infectious viruses in their lungs. Without peptide treatment (DMSO) and at 24, 48, and 120 h postinfection, infectious virus titers reached 10^6, $10^{6.75}$, and $10^{6.82}$ $TCID_{50}$s/ml, respectively. In contrast, after treatment of mice with 20, 200, or 500 μM z-LVLQTM-fmk, virus titers dropped to $10^{4.2}$ to 10^5 $TCID_{50}$s/ml for all the conditions tested. To confirm replication, an additional experiment was performed where mice were infected and lungs were harvested either immediately or at 48 h postinfection and then subjected to viral titrations (Fig. 8B). Results showed that the inoculum was totally recovered in the lungs of infected mice at day 0 postinoculation. When lungs were harvested at 48 h postinfection, the viral titer significantly increased, thus showing that viral replication indeed occurred after infection of the mice. In addition, the z-LVLQTM-fmk-mediated inhibition was specific since this peptide also impaired virus replication compared to the unrelated control peptide z-FA-fmk at 48 h postinfection (Fig. 8B). More importantly, when administration of the peptide was performed at 12 h postinfection, inhibition of viral replication was also readily detectable (Fig. 8C). The viral titers from control-treated animals reached $10^{6.53}$ $TCID_{50}$s/ml, while the viral titer of z-LVLQTM-fmk-treated animals was $10^{4.08}$ $TCID_{50}$s/ml at 48 h postinfection. Altogether, these results suggested that LVLQTM inhibited virus replication *in vivo* and could be of particular interest for anti-HRV therapies.

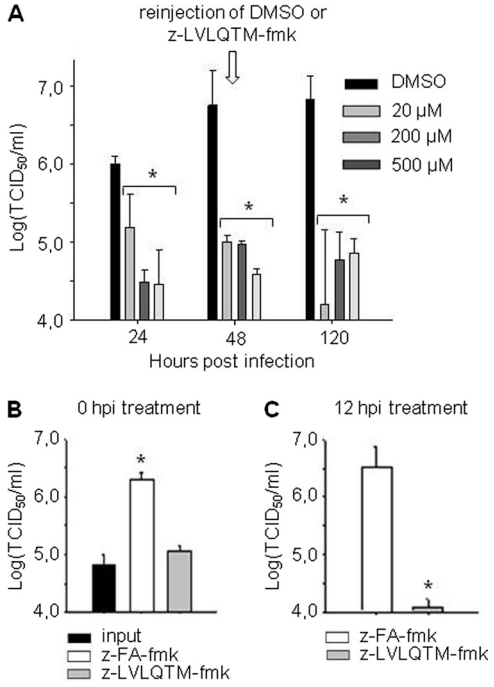

FIG 8 z-LVLQTM-fmk specifically inhibits HRV replication *in vivo*. (A) Mice were inoculated intranasally with 100,000 PFU HRV-2 per mouse (in a 25-μl volume) and treated with additional 25 μl of a solution containing the indicated concentrations of peptide or 1% DMSO. Lungs of infected mice were harvested at 24, 48, and 120 h postinfection, and virus titers were determined. (B) Mice were infected with HRV-2 as described above and treated with 20 μM z-LVLQTM-fmk or z-FA-fmk (control peptide). Lungs of infected mice were harvested immediately (input) or at 48 h postinfection (hpi). Virus titers were determined as described in Materials and Methods. (C) Mice were infected with HRV-2 (100,000 PFU) and treated with 20 μM z-LVLQTM-fmk or z-FA-fmk at 12 h postinfection. Lungs of infected mice were harvested at 48 h postinfection and virus titers were measured. *, $P < 0.05$.

DISCUSSION

Rhinoviruses are responsible for a large number of respiratory tract infections which range from the common cold to more serious complications, such as pneumonia, bronchitis, or bronchiolitis in children as well as in adults. These infections constitute a major public health problem and have a significant socioeconomic impact due to the fact that there is currently no effective drug to fight against HRV. In the search for an effective treatment against rhinovirus, we identified a peptide inhibitor of the viral 2A^{pro} by a yeast two-hybrid screening. This high-throughput screening allowed us to successfully identify 10 different peptides that were nonhydrolyzable by the 2A protease. Based on their sequence analysis, we postulated that these peptides could bind to the protease in a substrate-like manner (lock-and-key model). Direct evidence of peptide binding to the protease was provided by the protease-Glo assay, which elected the sequence motif LVLQTM derived from the very C terminus of the RBM6Δ6 protein to be the best candidate for subsequent development as an irreversible inhibitor of 2A^{pro}. This peptide had the following main features: (i) it specifically bound *in vitro* to the HRV-2 2A^{pro}, as demonstrated by pulldown assays. (ii) Its strong similarity to the amino-terminal half of natural cleavage sites of the protease meant that this motif behaved *in vitro* as a perfect pseudosubstrate not only of HRV-2 2A^{pro} but also

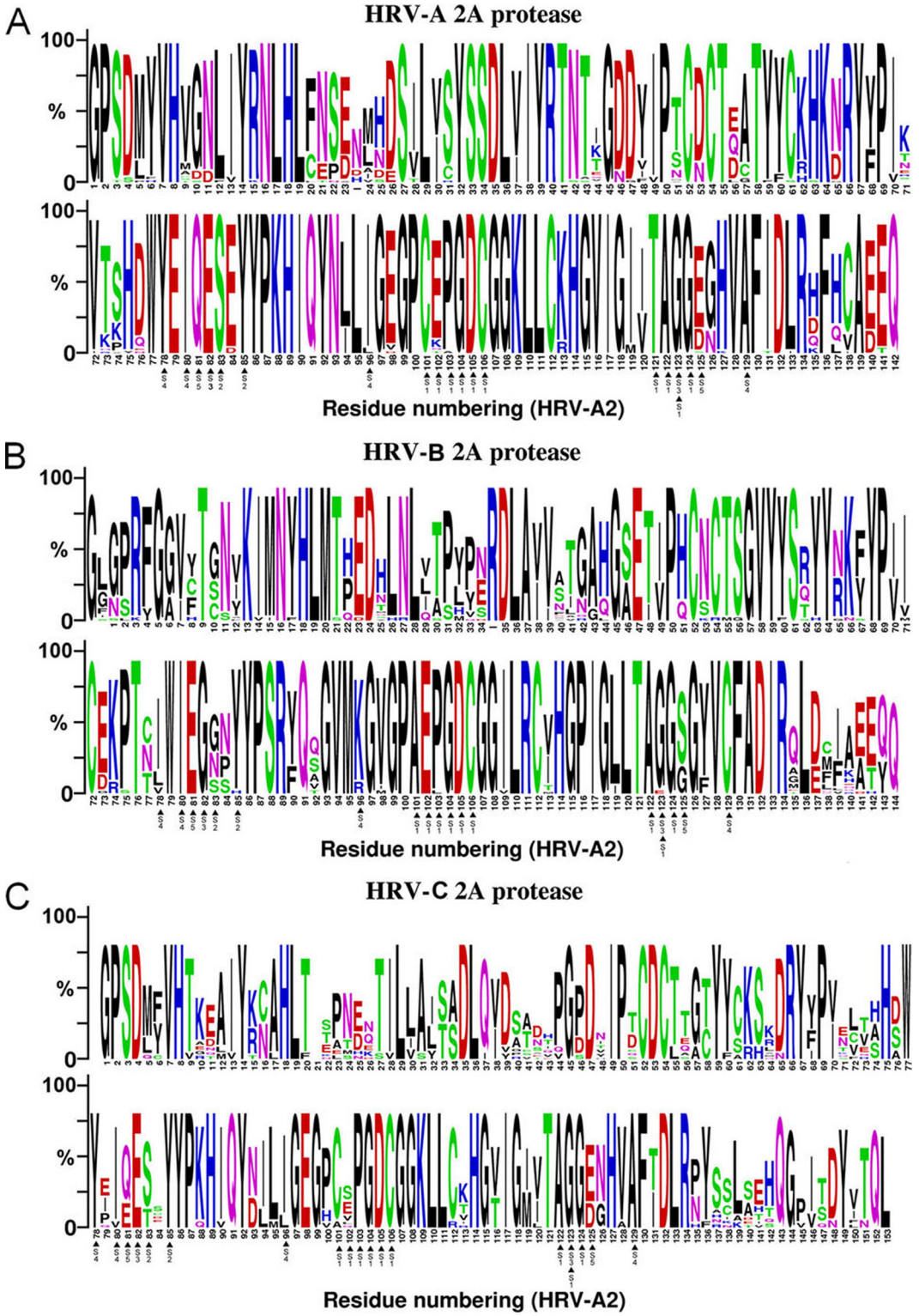

FIG 9 WebLogo sequence based on alignments of HRV type A, B, and C 2A proteases. These WebLogo sequences were generated using the WebLogo sequence generator (4) at http://weblogo.berkeley.edu/logo.cgi and were created using an alignment of 40 HRV-A sequences (A1, A2, A7, A9, A10, A11, A12, A13, A15, A16, A23, A24, A28, A29, A30, A34, A36, A38, A39, A41, A44, A46, A49, A53, A55, A56, A59, A64, A73, A74, A75, A76, A78, A82, A88, A89, A94, A101, A102, and A103) (A), 25 HRV-B sequences (B3, B4, B5, B6, B14, B17, B26, B27, B35, B37, B42, B48, B52, B69, B70, B72, B79, B83, B84, B86, B91, B92, B93, B97, and B99) (B), and 12 HRV-C sequences (C1 to C11 and C15) (C). The letter size is proportional to the degree of amino acid conservation, and arrows indicate residues involved in the binding of the LVLQTM peptide at subsites S5 to S1.

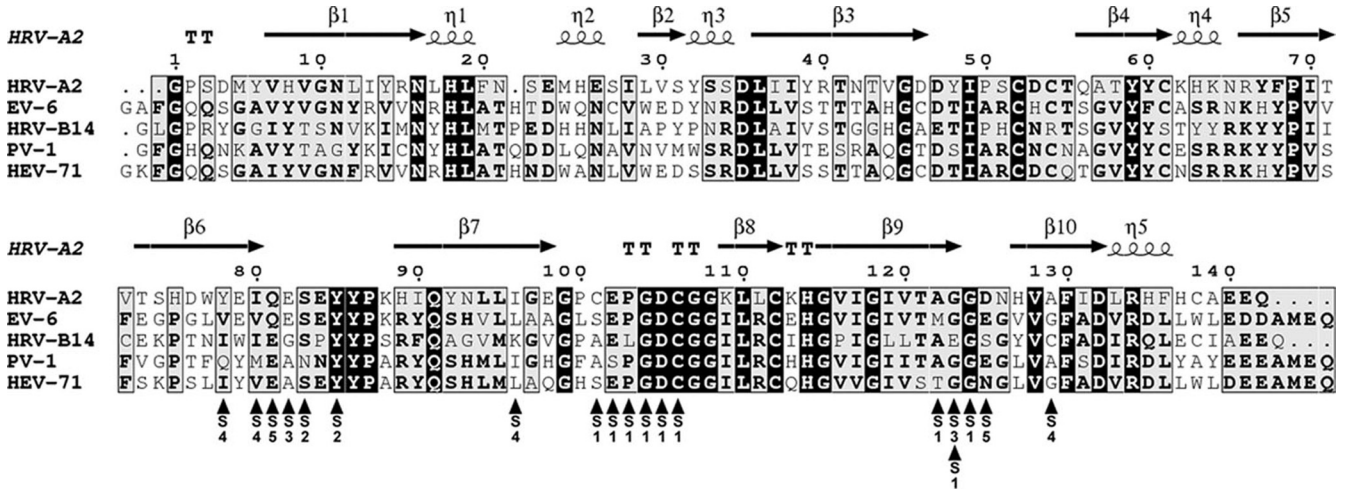

FIG 10 Multiple-sequence alignments of enterovirus 2A^{pro}. Sequence alignment was performed using the ClustalW program and plotted with the ESPript program (8). Similar residues are highlighted in gray; identical residues are in black. Secondary structure elements of HRV-2 2A^{pro} are shown above the sequences, while arrows indicate residues involved in the binding of the VLQTM peptide at subsites S5 to S1.

of EV-6 2A^{pro}, another enteroviral 2A protease. These enzymes share a relatively low level of amino acid sequence identity (40%), leading to substantially different surface characteristics, and thus represent two extremes in the primary sequence diversity of the 2A^{pro} family. (iii) It contained a P1 Met which was demonstrated to enhance significantly the binding affinity of the peptide for the enzyme (4, 28).

Therefore, our results support a molecular model whereby the C terminus of RBM6Δ6, acting as a competitive inhibitor of 2A^{pro}, docks into the substrate-binding pocket of the enzyme. Notably, in their screening of a HeLa cell cDNA expression library by the yeast two-hybrid procedure, Ventoso et al. (1999) (33) had previously characterized several four-amino-acid-binding peptides that interfered *in vitro* with PV-1 2A^{pro} activity. However, our data indicate that compared to its shorter version, LQTM, the LVLQTM sequence confers higher binding affinity to RBM6Δ6 for 2A^{pro}. These results thus highlighted the benefit which may be gained by using 6-mer-based peptides instead of 4-mer-based compounds directed against HRV 2A^{pro}.

To achieve a more potent inhibition of the 2A^{pro}, the LV LQTM peptide was modified so that it contained an electrophilic group (fmk) to enable the formation of a covalent bond with the active-site thiol and a benzyloxycarbonyl group (z) to increase its cell permeation. So modified, the z-LVLQTM-fmk compound was an effective inhibitor of purified HRV-2 2A^{pro} activity with a K_i value of 0.3 μM, which is about 20 times lower than that of the CBV 2A^{pro} inhibitor z-IETD-fmk (K_i = 7.7 μM) (1) and the caspase inhibitor z-VAD-fmk, which is also active against HRV 2A^{pro} (K_i = 5.6 μM) (5). Then we showed that z-LVLQTM-fmk specifically inhibited HRV-2 replication *in vitro* in A549 cells but also *in vivo* in BALB/c mice. The mouse model has features very similar to those observed in rhinovirus infection in humans, including augmentation of allergic airway inflammation (2), and to our knowledge, our study is the first one to validate *in vivo* in mice an antiviral drug directed against HRV. Mouse infection by HRV-2 was made possible by the fact that this virus strain, which belongs to the minor HRV group, uses a member of the low-density-lipoprotein receptor family and can bind the mouse counterpart. Moreover, direct injection of the peptide by the intranasal route in mice several hours after infection prefigures the outline for administration of a drug that could be used in humans for efficient anti-HRV therapy.

On the basis of HRV-2 2A^{pro} crystallographic data, a virtual docking model was then proposed to predict the inhibitor binding mode into the ligand binding pocket of the enzyme. Sequence comparison between different 2A^{pro} enzymes from HRV-A, -B, and -C species revealed that amino acid residues involved in the interaction with the inhibitor in our model are relatively well conserved.

The alignment of 40 HRV-A 2A^{pro} sequences (Fig. 9A) shows that for eight serotypes analyzed, Ile96 is replaced by a Leu, which displays the same physicochemical properties and so likely mediates the same hydrophobic interactions with P4 Leu. Interestingly, Asp125 found in 10 serotype sequences is replaced by a Glu, whose longer side chain may enhance a major interaction with P5 Val. Concerning the 25 HRV-B 2A proteins analyzed (Fig. 9B), hydrophobic interactions with P4 Leu are conserved through hydrophobic residues Ile, Leu, and Val at position 78. Ser83, which appears to be crucial for interaction with P3 Gln, is poorly conserved in type B sequences, as a Gly and an Asn are found at 50% and 35%, respectively. The second highlighted interaction through Asp125 also seems to be weakened in type B, as a serine is generally found at this position. Basic residues Arg and Lys are found at position 96, probably changing interaction modalities with the hydrophobic P4 Leu; nevertheless, the peptide LVLQTM seems to well accommodate in the catalytic cleft, even though a Lys is found at position 96 in HRV-B14. On the other hand, the Cys at position 129 (A129 in HRV-A2 2A^{pro}) found in all type B sequences may reinforce the hydrophobic interaction with P4 Leu. Finally, I80V, S83T, I96L, C101A, and D125E mutations occurring in only a few type C sequences (Fig. 9C) should have no detrimental effects on the interaction between the enzyme and its inhibitor, as they represent conservative mutations from a physicochemical point of view.

If our peptide inhibitor may be of general use against all HRV serotypes, its use for therapeutic purposes could be extended to other enterovirus-associated diseases since it is also active against poliovirus 1 (PV-1; GenBank accession number VO1149) and human enterovirus 71 (HEV-71; GenBank accession number AEF32490) 2A proteases (data not shown). Comparison of the sequences of these proteases with those of other proteases tested in this study for their interaction with LVLQTM reveals only minor differences (Fig. 10). In particular, S5 Gln81 is present in EV-6, while a similar glutamate is found in the other viruses. Asp125 properties are conserved through the glutamate or the asparagine in EV-6 and PV-1 or HEV-71, respectively. The serine at the same position in HRV-B14 with a side chain shorter than Asp and obviously shorter than Glu may reflect some flexibility of the substrate at P5, where it is largely solvent exposed (Fig. 5A). The apolar depression defining S4 is conserved, as all residues at positions 78, 80, 96, and 129, even though they are not similar, are hydrophobic, except for PV-1 at Gln78 and HRV-B14 at Lys96. Glu82 and Gly123 at S3 are not well conserved, but peptide interactions occur through their backbone; this would not have any consequences on affinity. Tyr85 and Ser83 are strictly conserved at S2, except PV-1 displays a glutamine at position 83. Finally, the flat and narrow pocket displaying very good chemical complementarities to the P1 Met side chain is well conserved among the different viruses, as residues 101 to 106 and 122 to 124 as well as Tyr85 are homologous. Therefore, this model allows accurate prediction of the interaction of the peptide inhibitor with a large spectrum of 2A proteases. This model also suggests affinity differences between enteroviral 2A proteases for the LVLQTM peptide. In particular, the longer side chain of S4 I80 and S4 I96 in the HRV-2 2A protease compared to S4 V80 and S4 L96 in EV-6 $2A^{pro}$ (Fig. 10) might reinforce the Van der Waals interactions with the P4 L in the peptide inhibitor. Moreover, the presence of a hydrophobic cysteine 101 at position S1 in HRV-2 $2A^{pro}$ instead of a polar serine in EV-6 $2A^{pro}$ likely strengthens the interaction with the P1 methionine in the peptide inhibitor. Such predictions could thus account for the better affinity of HRV-2 $2A^{pro}$ for the LVLQTM peptide compared to the EV-6 $2A^{pro}$, as confirmed by our experimental data (compare Fig. 5a and d).

From a more fundamental point of view, this study also highlights several clues concerning the exact role, if any, played by the RBM6Δ6 protein in the context of virus-infected cells. One possibility is that RBM6Δ6 is an antidote molecule which is expressed by the cell in response to viral infection and which specifically neutralizes protein poison $2A^{pro}$. Conversely, and more likely, binding of the protease on RBM6Δ6 could have a more or less profound impact on normal function of this protein in favor of viral infection. Experiments are under way to try to resolve this new and very exciting enigma.

ACKNOWLEDGMENTS

We thank Monique Ballandras for technical assistance as well as Leslie C. Sutherland and Sophie Bonnal for providing a plasmid encoding the full-length RBM6 protein.

This project was supported by the National Reference Center of Enteroviruses, the Institut de Veille Sanitaire, and the Agence Nationale de la Recherche (ANR; to Béatrice Riteau).

The funders had no role in study design, data collection and analysis, decision to publish, or preparation of the manuscript.

We declare no competing financial interests.

REFERENCES

1. **Badorff C, et al.** 2000. Enteroviral protease 2A directly cleaves dystrophin and is inhibited by a dystrophin-based substrate analogue. J. Biol. Chem. **275**:11191–11197.
2. **Bartlett NW, et al.** 2008. Mouse models of rhinovirus-induced disease and exacerbation of allergic airway inflammation. Nat. Med. **14**:199–204.
3. **Belov GA, et al.** 2000. Early alteration of nucleocytoplasmic traffic induced by some RNA viruses. Virology **275**:244–248.
4. **Deszcz L, Cencic R, Sousa C, Kuechler E, Skern T.** 2006. An antiviral peptide inhibitor that is active against picornavirus 2A proteinases but not cellular caspases. J. Virol. **80**:9619–9627.
5. **Deszcz L, Seipelt J, Vassilieva E, Roetzer A, Kuechler E.** 2004. Antiviral activity of caspase inhibitors: effect on picornaviral 2A proteinase. FEBS Lett. **560**:51–55.
6. **Fromont-Racine M, Rain JC, Legrain P.** 1997. Toward a functional analysis of the yeast genome through exhaustive two-hybrid screens. Nat. Genet. **16**:277–282.
7. **Garcia-Calvo M, et al.** 1998. Inhibition of human caspases by peptide-based and macromolecular inhibitors. J. Biol. Chem. **273**:32608–32613.
8. **Gouet P, Robert X, Courcelle E.** 2003. ESPript/ENDscript: extracting and rendering sequence and 3D information from atomic structures of proteins. Nucleic Acids Res. **31**:3320–3323.
9. **Gustin KE, Sarnow P.** 2002. Inhibition of nuclear import and alteration of nuclear pore complex composition by rhinovirus. J. Virol. **76**:8787–8796.
10. **Joachims M, Van Breugel PC, Lloyd RE.** 1999. Cleavage of poly(A)-binding protein by enterovirus proteases concurrent with inhibition of translation in vitro. J. Virol. **73**:718–727.
11. **Jurgens CK, et al.** 2006. 2Apro is a multifunctional protein that regulates the stability, translation and replication of poliovirus RNA. Virology **345**:346–357.
12. **Kempf BJ, Barton DJ.** 2008. Poliovirus 2A(Pro) increases viral mRNA and polysome stability coordinately in time with cleavage of eIF4G. J. Virol. **82**:5847–5859.
13. **Khoufache K, et al.** 2009. Protective role for protease-activated receptor-2 against influenza virus pathogenesis via an IFN-gamma-dependent pathway. J. Immunol. **182**:7795–7802.
14. **Kistler A, et al.** 2007. Pan-viral screening of respiratory tract infections in adults with and without asthma reveals unexpected human coronavirus and human rhinovirus diversity. J. Infect. Dis. **196**:817–825.
15. **Konig H, Rosenwirth B.** 1988. Purification and partial characterization of poliovirus protease 2A by means of a functional assay. J. Virol. **62**:1243–1250.
16. **Laine P, Savolainen C, Blomqvist S, Hovi T.** 2005. Phylogenetic analysis of human rhinovirus capsid protein VP1 and 2A protease coding sequences confirms shared genus-like relationships with human enteroviruses. J. Gen. Virol. **86**:697–706.
17. **Lamphear BJ, et al.** 1993. Mapping the cleavage site in protein synthesis initiation factor eIF-4 gamma of the 2A proteases from human coxsackievirus and rhinovirus. J. Biol. Chem. **268**:19200–19203.
18. **Molla A, Hellen CU, Wimmer E.** 1993. Inhibition of proteolytic activity of poliovirus and rhinovirus 2A proteinases by elastase-specific inhibitors. J. Virol. **67**:4688–4695.
19. **Ohlmann T, Rau M, Pain VM, Morley SJ.** 1996. The C-terminal domain of eukaryotic protein synthesis initiation factor (eIF) 4G is sufficient to support cap-independent translation in the absence of eIF4E. EMBO J. **15**:1371–1382.
20. **Otto HH, Schirmeister T.** 1997. Cysteine proteases and their inhibitors. Chem. Rev. **97**:133–172.
21. **Palmenberg AC, et al.** 2009. Sequencing and analyses of all known human rhinovirus genomes reveal structure and evolution. Science **324**:55–59.
22. **Papi A, et al.** 2006. Infections and airway inflammation in chronic obstructive pulmonary disease severe exacerbations. Am. J. Respir. Crit. Care Med. **173**:1114–1121.
23. **Park N, Katikaneni P, Skern T, Gustin KE.** 2008. Differential targeting of nuclear pore complex proteins in poliovirus-infected cells. J. Virol. **82**:1647–1655.
24. **Petersen JF, et al.** 1999. The structure of the 2A proteinase from a common cold virus: a proteinase responsible for the shut-off of host-cell protein synthesis. EMBO J. **18**:5463–5475.

25. **Prevot D, et al.** 2003. Characterization of a novel RNA-binding region of eIF4GI critical for ribosomal scanning. EMBO J. **22**:1909–1921.
26. **Reed LJ, Muench H.** 1938. A simple method of estimating 50 per cent endpoints. Am. J. Hyg. **27**:493–497.
27. **Sommergruber W, et al.** 1994. 2A proteinases of coxsackie- and rhinovirus cleave peptides derived from eIF-4 gamma via a common recognition motif. Virology **198**:741–745.
28. **Sommergruber W, et al.** 1992. Cleavage specificity on synthetic peptide substrates of human rhinovirus 2 proteinase 2A. J. Biol. Chem. **267**: 22639–22644.
29. **Soto Rifo R, Ricci EP, Decimo D, Moncorge O, Ohlmann T.** 2007. Back to basics: the untreated rabbit reticulocyte lysate as a competitive system to recapitulate cap/poly(A) synergy and the selective advantage of IRES-driven translation. Nucleic Acids Res. **35**:e121.
30. **Studier FW.** 2005. Protein production by auto-induction in high density shaking cultures. Protein Expr. Purif. **41**:207–234.
31. **Timmer T, et al.** 1999. A comparison of genomic structures and expression patterns of two closely related flanking genes in a critical lung cancer region at 3p21.3. Eur. J. Hum. Genet. **7**:478–486.
32. **van Gunsteren WF.** 1996. Biomolecular simulation: the GROMOS96 manual and user guide. vdf, Zürich, Switzerland.
33. **Ventoso I, Barco A, Carrasco L.** 1999. Genetic selection of poliovirus 2Apro-binding peptides. J. Virol. **73**:814–818.
34. **Vojtek AB, Hollenberg SM.** 1995. Ras-Raf interaction: two-hybrid analysis. Methods Enzymol. **255**:331–342.
35. **Zunszain PA, et al.** 2010. Insights into cleavage specificity from the crystal structure of foot-and-mouth disease virus 3C protease complexed with a peptide substrate. J. Mol. Biol. **395**:375–389.